5th International Conference on Electrical and Computer Engineering
ICECE 2008, 20-22 December 2008, Dhaka, Bangladesh

Modeling and Numerical Analysis of Thermal Treatment of Granulated Porous Particles by Induction Plasma

M. Mofazzal Hossain[1], Y. Yao[2], M. Rafiqul Alam[3], M. Maksud Alam[3] and T. Watanabe[4]*

[1]Department of Electronics & Communications Engineering, East West University, Dhaka
[2] Kunming University of Science & Technology, Kunming 650093, Yunnan Province, China
[3]Chittagong University of Engineering & Technology, Chittagong-4349
[4]Tokyo Institute of Technology, G1-22, 4259 Nagatsuta, Yokohama 226-8502, Japan

*E-mail: dmmh@ewubd.edu

Abstract - In this paper it is aimed to describe the modeling and numerical analysis of thermal treatment of granulated porous particles by induction plasma. To investigate the heat exchange dynamics between plasma and particles during the flight of granulated porous particles through the hot plasma, a plasma-particle interactive flow model has been developed. This model solves the conservation equations to predict the temperature and flow fields of plasma, under local thermal equilibrium (LTE) conditions, and then computes the injected particles trajectories, temperature and size histories, and the particle source terms to incorporate the particle loading effects. It is found that the size and dose of injected particles greatly affect the particle trajectory and temperature, and hence the heat transfer to particles at higher powder feed-rate.

I. Introduction

Induction thermal plasma (ITP) has extensively been used for the synthesis and treatment of micro-particles since couple of decades as a clean reactive heat source [1]. Thermal plasma synthesis offers a versatile, cost-effective technology for the industrial-scale production of many advanced materials for demanding applications in high tech industries. The need for materials with improved physical and mechanical properties for demanding applications has gradually been increasing in such high tech industries as electronics, transportation, glass and nuclear power. ITP technology ensures essentially the in-flight, single-step, short time, and less pollution compared with the traditional technologies that have been using in the industries for the thermal treatment of granulated porous micro-particles. The thermal treatment of injected particles depends mainly on the plasma-particle heat exchange efficiency, which in turn depends to a large extent on the plasma temperature, particles trajectories, temperature and diameter histories. Experimentally, it is quite difficult to measure the particles trajectories, temperature and diameter histories during the flight through the hot plasma. Thus, the prediction of particles trajectories, temperature and diameter histories through numerical modeling is the prime concern. Boulos [2] developed a model and discussed the plasma-particle heat exchange dynamics for argon plasma. However, the particle porosity and its consequences during flight of the particle in the plasma were not discussed. The aim of this work is to demonstrate the modeling and simulation of the plasma-particle interactive flow in argon-oxygen plasma, for highly porous granulated micro-particles to optimize the discharge parameters that affect the treated particles diameter and compositions.

II. Modeling

Induction plasma is usually generated by radio frequency alternating current supply through some coils that surround a coaxial quartz tube and injecting plasma gas such as argon and sometimes mixtures of argon and molecular gases like oxygen, hydrogen, nitrogen etc. The discharged plasma flow can be treated as neutral fluid flow, although plasma itself is ionized, but it is electrically neutral. Again, for the thermal treatment of micro-particles, particles are injected into the plasma torch along with the carrier gas. Injected particles, penetrate the hot core of plasma, interact with that and exchange energy with plasma and get thermal treatment. Finally, treated particles are collected at the reaction chamber. Thus, to characterize the plasma-particle interaction behavior and to predict the plasma and particle parameters, that affect the size and morphology of the treated particles, we need to develop the plasma model and particle model, and correlate their interactions.

A. Plasma Model

The schematic geometry and dimensions of a typical ITP torch is presented in Fig.1 and Table 1 respectively. It is assumed that the plasma flow is 2-dimensioanl, axi-symmetric, laminar, steady, optically thin, and electromagnetic fields are 2-dimensional. With these assumptions the plasma flow is modeled by the conservation equations (1)-(4) and vector potential form of Maxwell's equation (5) [3]. This model solves the

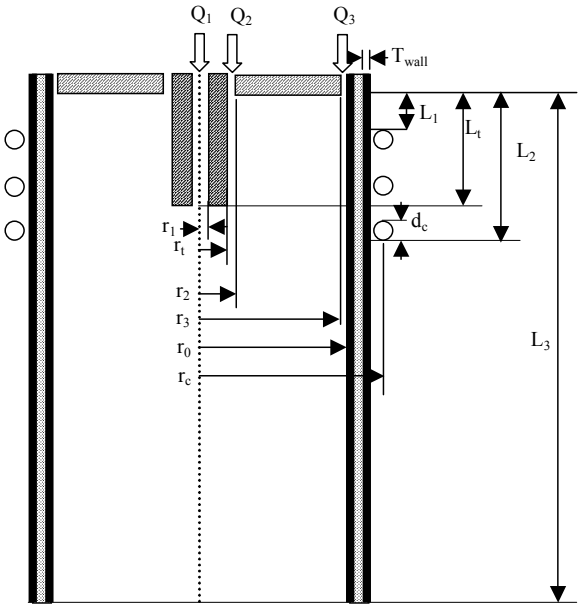

Fig.1 Schematic geometry and dimensions of ITP torch

conservation equations and vector potential form of Maxwell's equations simultaneously under LTE conditions, including a metal tube inserted into the torch. Adding the source terms to the conservation equations, the plasma-particle interaction and loading effects of particles injected into the torch, has been taken into account.

Mass conservation:

$$\nabla \cdot \rho \mathbf{u} = S_p^C \tag{1}$$

Momentum conservation:

$$\rho \mathbf{u} \cdot \nabla \mathbf{u} = -\nabla p + \nabla \cdot \mu \nabla \mathbf{u} + \mathbf{J} \times \mathbf{B} + S_p^M \tag{2}$$

Energy conservation:

$$\rho \mathbf{u} \cdot \nabla h = \nabla \cdot \left(\frac{\kappa}{C_p} \nabla h \right) + \mathbf{J} \cdot \mathbf{E} - Q_r - S_p^E \tag{3}$$

Species conservation:

$$\rho \mathbf{u} \cdot \nabla y = \nabla \cdot \left(\rho D_m \nabla y \right) + S_p^C \tag{4}$$

Vector potential form of Maxwell field equation [3]:

$$\nabla^2 \mathrm{A_c} = i \mu_0 \sigma \omega \mathrm{A_c} \tag{5}$$

Where, ∇: vector operator, $\mathbf{u}$: velocity vector, ρ: mass density, μ: viscosity, σ: electrical conductivity, κ: thermal conductivity, h: enthalpy, p: pressure, C_p: specific heat at constant pressure, D_m: multicomponent diffusion coefficient, y: mass fraction, $\mathbf{J}$: current density vector, $\mathbf{E}$: electric field vector, $\mathbf{B}$: magnetic field vector, Q_r: volumetric radiation loss, $\mathrm{A_c}$: complex amplitude of vector potential, μ_0: permeability of free space, ω: $2\pi f$ (f: frequency), i: complex vector ($\sqrt{-1}$). The particle source terms S_p^C, S_p^M and S_p^E are the contributions of particles to the mass and species, momentum and energy conservation equations respectively.

Table 1: Torch dimensions

Distance to initial coil position (L_1)	19 mm
Length of injection tube (L_t)	52 mm
Distance to end of coil position (L_2)	65 mm
Torch length (L_3)	190 mm
Coil diameter (d_c)	5 mm
Wall thickness of quartz tube (T_{wall})	1.5 mm
Inner radius of injection tube (r_1)	1 mm
Outer radius of injection tube (r_t)	4.5 mm
Outer radius of inner slot (r_2)	6.5 mm
Inner radius of outer slot (r_3)	21.5 mm
Torch radius (r_0)	22.5 mm
Coil radius (r_c)	32 mm

The boundary conditions, thermodynamic and transport properties of argon and oxygen gases are the same as those described in our previous work [4].

B. Particle Model

The following assumptions are made in the analysis of plasma-particle interactions: (i) the particle motion is two-dimensional; (ii) only the viscous drag force and gravity affect the motion of an injected particle; (iii) the temperature gradient inside the particle is neglected; (iv) the particle charging effect caused by the impacts of electrons or positive ions is negligible; (v) the electromagnetic drag forces caused by the particle charging of the injected particles are negligible compared with those by neutrals and charged particles. Thus, the momentum equations for a single spherical particle injected vertically downwards into the plasma torch can be expressed by equations (6), (7) and (8).

$$\frac{du_p}{dt} = -\frac{3}{4} C_D (u_p - u) U_R \left(\frac{\rho}{\rho_p d_p} \right) + g \tag{6}$$

$$\frac{dv_p}{dt} = -\frac{3}{4} C_D (v_p - v) U_R \left(\frac{\rho}{\rho_p d_p} \right) \tag{7}$$

$$U_R = \sqrt{(u_p - u)^2 + (v_p - v)^2} \tag{8}$$

The particle temperature, liquid fraction and particle diameter are predicted according to the energy balance equations (9), (10), (11) and (12).

$$Q = \pi d_p^2 h_c \left(T - T_p \right) - \pi d_p^2 \sigma_s \varepsilon \left(T_p^4 - T_a^4 \right) \tag{9}$$

$$\frac{dT_p}{dt} = \frac{6Q}{\pi \rho_p d_p^3 C_{pp}}, \quad T_p < T_b \tag{10}$$

$$\frac{dx}{dt} = \frac{6Q}{\pi \rho_p d_p^3 H_m}, \; 1000 \le T_p \le 1600 \tag{11}$$

$$\frac{dd_p}{dt} = -\frac{2Q}{\pi \rho_p d_p^2 H_v}, \; 1000 \le T_p \le 1600, \; T_p \ge T_b \tag{12}$$

Where u_p: axial velocity component of particle, v_p: radial velocity component of particle, g: acceleration of gravity,

ρ_p: particle mass density, d_p: particle diameter, Q: the net heat exchange between the particles and its surroundings, T_p and T_b: particle temperature and boiling point temperature, respectively, T: plasma temperature, T_a: ambient temperature, ε: particle surface emissivity; σ_s: Stefan-Boltzmann constant, C_{pp}: particle specific heat, H_m and H_v: latent heat of particle melting and vaporization respectively, and x: the liquid mass fraction of the particle. Drag coefficient C_{Df} is calculated using equation (13) and the property variation at the particle surface layer and the non-continuum effects are taken into account by equations (14) and (15) respectively [5].

$$C_{Df} = \begin{cases} \dfrac{24}{R_e} & R_e \le 0.2 \\ \dfrac{24}{R_e}\left(1+\dfrac{3}{16}R_e\right) & 0.2 < R_e \le 2.0 \\ \dfrac{24}{R_e}\left(1+0.11R_e^{\,0.81}\right) & 2.0 < R_e \le 21.0 \\ \dfrac{24}{R_e}\left(1+0.189R_e^{\,0.62}\right) & 21.0 < R_e \le 200 \end{cases} \quad (13)$$

$$f_1 = \left(\frac{\rho_\infty \mu_\infty}{\rho_s \mu_s}\right)^{-0.45} \quad (14)$$

$$f_2 = \left\{1+\left(\frac{2-\alpha}{\alpha}\right)\left(\frac{\gamma}{1+\gamma}\right)\frac{4}{Pr_s}Kn\right\}^{-0.45}, \; 10^{-2}<Kn<0.1 \quad (15)$$

$$C_D = C_{Df} f_1 f_2 \quad (16)$$

To take into account the steep temperature gradient between plasma and particle surface, the Nusselt correlation can be expressed by equation (17) [6]. The non-continuum effect is taken into account by equation (18) [5].

$$Nu_f = (2.0+0.6R_{ef}^{1/2}Pr_f^{1/3})\left(\frac{\rho_\infty \mu_\infty}{\rho_s \mu_s}\right)^{0.6}\left(\frac{C_{p\infty}}{C_{ps}}\right)^{0.38} \quad (17)$$

$$f_3 = \left\{1+\left(\frac{2-\alpha}{\alpha}\right)\left(\frac{\gamma}{1+\gamma}\right)\frac{4}{Pr_s}Kn\right\}^{-1}, \; 10^{-3}<Kn<0.1 \quad (18)$$

The convective heat transfer coefficient is predicted by equation (19).

$$h_{cf} = \frac{\kappa_f}{d_p} Nu_f f_3 \quad (19)$$

In the above expressions, subscript f, ∞ and s refer to properties corresponding to the film temperature (arithmetic mean of plasma and particle temperatures), plasma temperature and particle temperature respectively, C_p: particle specific heat, h_c: heat transfer coefficient, Nu: Nusselt number, Pr: Prandtl number, Re: Reynold number, $\propto$: thermal accommodation coefficient, γ: specific heat ratio and Kn: Knudsen number. The physical properties of soda-lime glass powders are: mass density 2300 kg-m^{-3}, specific heat 800 J-kg^{-1}K^{-1}, surface emissivity 80%, fusion and boiling temperature 1000~1600 K and 2500 K respectively, heat of fusion, and vaporization 3.69×10^5 J-kg^{-1} and 1.248×10^7 J-kg^{-1}, respectively.

C. Particle Source Terms

To take into account the particle loading effects the particle source terms for the mass, momentum, energy and species conservation equations have been calculated using the PSI-Cell (Particle-Source-In Cell) approach [7], where the particles are regarded as sources of mass, momentum and energy.

Let us assume N_t^0 is the total number of particles injected per unit time, n_d is the particle size distribution, and n_r is the fraction of N_t^0 injected at each point through the injection nozzle. Thus, the total number of particles per unit time traveling along the trajectory (l,k) corresponding to a particle diameter d_l injected at the inlet point r_k can be expressed by equation (20).

$$N^{(l,k)} = n_{d_l} n_{r_k} N_t{}^0 \quad (20)$$

The source terms in the mass and species conservation equation, S_p^C is the net flux rate of particles mass in a computational cell (control volume). Assuming the particles are spherical, the flux rate of particle mass for the particle trajectory (l,k) that traverses a given cell (i, j) can be expressed by equation (21).

$$S_{p,ij}^{C(l,k)} = \frac{1}{6}\pi\rho_p N_{ij}^{(l,k)}(d_{ij,in}^3 - d_{ij,out}^3) \quad (21)$$

The net flux rate of particle mass is obtained by summing over all particles trajectories which traverse a given cell (i, j) by equation (22).

$$S_{p,ij}^C = \sum_l \sum_k S_{p,ij}^{C(l,k)} \quad (22)$$

The source terms for axial and radial momentum conservation equations are evaluated in the same fashion as that of mass conservation equation. In this case, the flux rate of particles momentum for the particle trajectory (l,k) traversing a given cell (i, j) is expressed by equations (23) and (24).

$$S_{p,ij}^{M_z(l,k)} = \frac{1}{6}\pi\rho_p N_{ij}^{(l,k)}(u_{ij,in}d_{ij,in}^3 - u_{ij,out}d_{ij,out}^3) \quad (23)$$

$$S_{p,ij}^{M_r(l,k)} = \frac{1}{6}\pi\rho_p N_{ij}^{(l,k)}(v_{ij,in}d_{ij,in}^3 - v_{ij,out}d_{ij,out}^3) \quad (24)$$

Thus, the corresponding source terms for axial and radial momentum conservation equations can be expressed by equations (25) and (26) respectively.

$$S_{p,ij}^{M_z} = \sum_l \sum_k S_{p,ij}^{M_z(l,k)} \quad (25)$$

$$S_{p,ij}^{M_r} = \sum_l \sum_k S_{p,ij}^{M_r(l,k)} \quad (26)$$

The source term for energy conservation equation $S_{p,ij}^{E}$ consists of the heat given to the particles $Q_{p,ij}^{(l,k)}$, and superheat to bring the particle vapors into thermal equilibrium with the plasma $Q_{v,ij}^{(l,k)}$, and these terms are expressed by equations (27), (28) and (29).

$$Q_{p,ij}^{(l,k)} = \int_{\tau_{in}}^{\tau_{out}} \pi d_p^{\,2} h_c (T_{ij} - T_{p,ij}^{(l,k)}) dt \quad (27)$$

$$Q_{v,ij}^{(l,k)} = \int_{\tau_{in}}^{\tau_{out}} \frac{\pi}{2} \pi d_p^{\,2} \rho_p \left(\frac{dd_p}{dt} \right) C_{pv} (T_{ij} - T_{p,ij}^{(l,k)}) dt \quad (28)$$

$$S_{p,ij}^{E} = \sum_l \sum_k N_{ij}^{(l,k)} (Q_{p,ij}^{(l,k)} + Q_{v,ij}^{(l,k)}) \quad (29)$$

D. Computation Methodology

For the sake of computation, the particle concentration in the inlet is assumed to be uniform and to be separated into five injection points, which are at radial positions of 0.3, 0.45, 0.6, 0.75 and 0.9 mm from the torch centerline. In the present computation the particles diameter distribution is assumed to be Maxwellian, and the powder is assumed to be composed of seven size particles according to its diameter and deviation. The average particle diameter is 58 μm and the maximum deviation is 67%. As a result, there are 35 different possible particle trajectories. The injection velocity of the particles is assumed to be equal to the initial velocity of the carrier gas. The described plasma and particle models are solved by developing a code using control volume algorithm [8]. Solving the plasma temperature and flow fields without injection of any particles starts the computation. Using these conversed temperature and flow fields, particles trajectories together with particle temperature and size histories are computed. The particle source terms for the mass, momentum and energy conservation equations for each control volume throughout the torch are then predicted. The plasma temperature and flow fields are predicted again incorporating these particle source terms. The new plasma temperature and flow fields are used to recalculate the particles trajectories, temperature and size histories. Computing the new source terms and incorporating them into conservation equations constitute the effects of plasma-particle interaction, thereby completing the cycle of mutual interaction. The above computation schemes are repeated until the convergence.

III. Simulated Results

The developed model is used to predict the plasma fields (e.g plasma temperature and flow velocity) and the energy exchange between plasma and particle, particle trajectories, and particle temperature and size histories along the trajectories. The present computation is carried out for soda-lime-silica glass particles. Computation is carried out for a plasma discharge of 10 kW plasma power, 4 MHz induction frequency and 0.1 MPa pressure. Fig.2 shows the effects of carrier gas flow-rate on the spatial plasma temperature. This figure clearly depicts that higher carrier gas flow-rate cools the plasma around the torch centerline and has insignificant effects away from the torch centerline. Also the higher the carrier gas flow-rate the lower the residence time of particles in plasma contact, due to the higher plasma velocity. Fig.3 shows the particle trajectories at 6 L-min^{-1} carrier gas flow-rate and 10 gm-min^{-1} powder feed-rate. It is noticed that particles having larger diameter remain close to the torch centerline and lighter particles move more away from the centerline. Fig.4 shows the particle temperature (for 20, 50 and 90 μm particles) computed from the energy balance equation. It is found that the smaller particle attains the boiling point temperature and larger

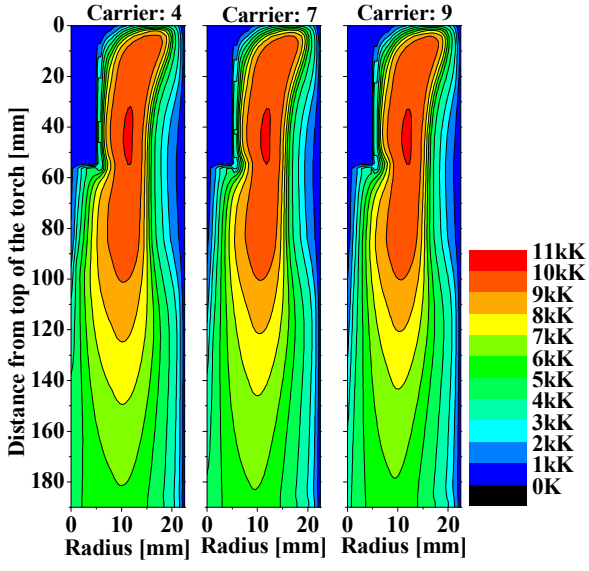

Fig.2 Effects of carrier gas on plasma isotherms

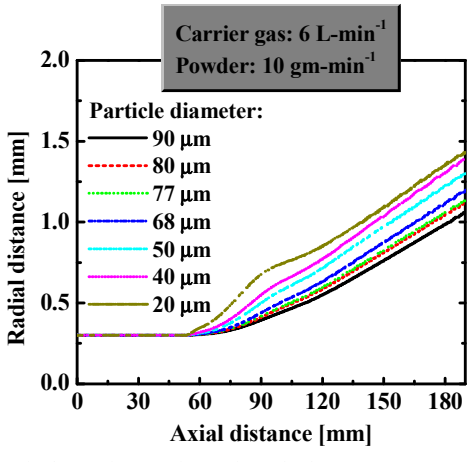

Fig.3 Particle trajectories within the plamsa torch

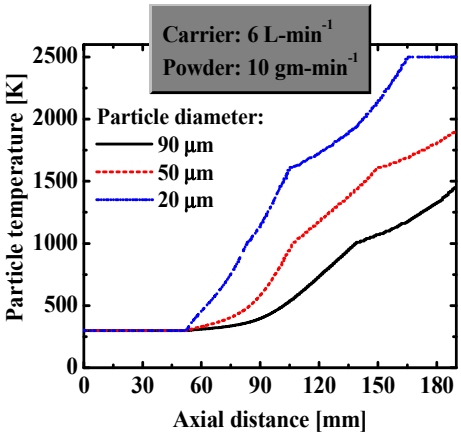

Fig.4 Dependence of particle temperature on diameter

particle attains low temperature. This is because, larger particles fly through the low temperature region (almost along the torch centerline) and smaller particles fly through the high temperature region away from the centerline as described in Fig.3. The porosity of particles is about 80%. The porous particles move through the plasma and gets heated and melted, thus the porosity becomes zero and particles become compact. After melting, particle temperature increases and reaches boiling point temperature and diameter starts to decrease due to vaporization. Thus, it is comprehended that diameter decreases due to the decrease of porosity and vaporization. Fig.5 shows the effects of carrier gas flow-rate on the diameter history within the torch for a particle of 20 μm diameter. For the solid curve diameter remains unchanged up to point A (melting starts), and then from A to B (melting completed) diameter shrinks due to the change of porosity, and from point C diameter changes due to the vaporization. Fig.6 displays the plasma and particle axial velocity. This figure depicts that the lighter particle (20 μm) has similar velocity as that of plasma, and larger particles attain high velocity in the downstream of plasma flow; although the larger particles have smaller velocity in the upstream of plasma flow due to their large inertia. Fig.7 describes the dependence of energy transfer to particles on diameter. It is noticed that energy transfer (per unit mass) to smaller particles is larger than that of larger particles. According to energy balance equations

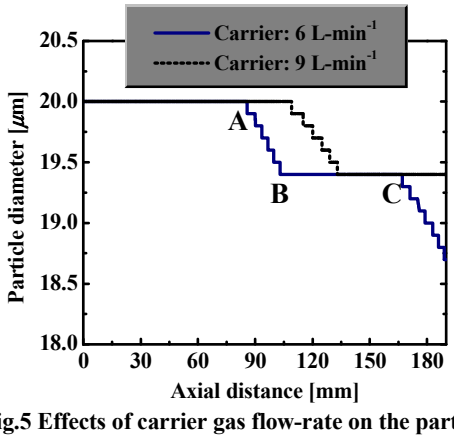

Fig.5 Effects of carrier gas flow-rate on the particle diameter history

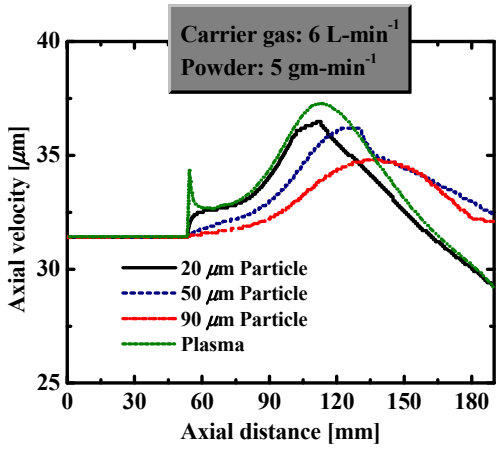

Fig.6 Axial velocity of particle with the plasma

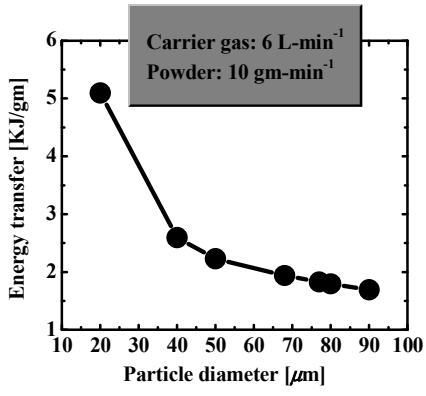

Fig.7 Dependence of energy transfer on particle diameter

(9) and (10), energy transfer to particles is dominated by the surface area of the particles. As the number of smaller particles is much larger than that of larger particles in per unit mass, thus total surface area is larger for smaller particles for per unit mass. These results are also supported by the previous results presented in Fig.4, where smaller particles attain higher temperature, because larger energy transfer to particles means higher particle temperature.

IV. Conclusions

A plasma-particle interactive flow model is described. This model may be used as a tool for the numerical analysis and simulation of any granulated porous micro-particles. The developed model can be used to optimize the carrier gas flow-rate, particle feed-rate, and particle size distribution to achieve the maximum treatment efficiency during thermal treatment of granulated porous particles by single or mixed-gas induction thermal plasmas. Numerically, it is found that the heat transfer to particles decreases at increased carrier gas flow-rate and energy transfer to smaller particles is higher than that of larger particles for per unit mass, and these results well agree with those of experiment [9]. Thus, it may be argued that the efficient thermal treatment of particles depends not only on the physical properties of the

particles, but also on the plasma discharge conditions and particle parameters.

References

[1] T. Watanabe and K. Fujiwara, "Nucleation and growth of oxide nanopartilces prepared by induction thermal plasmas," *Chem. Eng. Comm.,* vol. 191, pp.1343-1361, 2004.

[2] M. I. Boulos, "Heating of Powders in the Fire Ball of an Induction Plasma," *IEEE Tran.Plasma Sci.*, vol. PS-6, pp. 93- , 1978.

[3] J. Mostaghimi, K. C. Paul, and T. Sakuta, "Transient Responses of the Radio Frequency Inductively Coupled Plasma to a Sudden Change in Power", *J. Appl. Phys*., vol. 83, pp. 1898-1908 1998.

[4] M. M. Hossain, Y. Yao, Y. Oyamatsu, T. Watanabe, F. Funabiki and T. Yano, *WSEAS Trans. Heat and Mass Transfer*, vol. 1, 625 (2006).

[5] X. Chen and E. Pfender, "Effect of the Knudsen Number on Heat Transfer to a Particle Immersed into a Thermal Plasma," *Plasma Chem. Plasma Process*. vol. 3, pp. 97- , 1983.

[6] Y. C. Lee, Y. P. Chyou, and E. Pfender, "Particle Dynamics and Particle Heat and Mass Transfer in Thermal Plasmas. Part II. Particle Heat and Mass Transfer in Thermal Plasmas," *Plasma Chem. Plasma Process*., vol. 5, pp. 391-414, 1985.

[7] C. T. Crowe, M. P. Sharma, and D. E. Stock, "The Particle-Source-In Cell (PSI-CELL) Model for Gas-Droplet Flows", *J. Fluids Eng.*, vol. 99, pp.325-332, 1977.

[8] S. V. Patankar, *Numerical Heat Transfer and Fluid Flow*, Hemisphere, New York, 1980.

[9] Y. Yao, M. M. Hossain, Y. Oyamatsu, T. Watanabe, F. Funabiki and T. Yano, "Plasma-particle heat transfer mechanism for in-flight melting of powders in induction thermal plasmas," Proceedings of ASCHT07 1st Asian Symposium on Computational Heat Transfer and Fluid Flow, Xi'an, China, October 18-21, 2007, Paper No. ASCHT2007-069.

.